Journal of Applied Physics

Modeling diffusion length damage coefficient in GaAs and InGaP solar cells under electron irradiation

Cite as: J. Appl. Phys. **131**, 104503 (2022); https://doi.org/10.1063/5.0079456
Submitted: 21 November 2021 • Accepted: 18 February 2022 • Published Online: 11 March 2022

P. Bisht

Journal of Applied Physics ARTICLE scitation.org/journal/jap

Modeling diffusion length damage coefficient in GaAs and InGaP solar cells under electron irradiation

Cite as: J. Appl. Phys. **131**, 104503 (2022); doi: 10.1063/5.0079456
Submitted: 21 November 2021 · Accepted: 18 February 2022 ·
Published Online: 11 March 2022

P. Bisht[a)]

AFFILIATIONS

U R Rao Satellite Centre, HAL Old Airport Road, Vimanapura, Bengaluru, Karnataka 560017, India

Note: This paper is part of the Special Topic on Radiation Effects in Materials.
[a)]**Author to whom correspondence should be addressed:** bishtp4496@gmail.com

ABSTRACT

A method is proposed for calculating the diffusion length damage coefficient for minority carriers (K_L) in GaAs and InGaP solar cells under electron irradiation using the Shockley–Read–Hall (SRH) model for defect-assisted recombination. In the SRH model, the damage coefficient K_L is proportional to the product $k\sigma_c$, where k is the defect introduction rate under particle radiation and σ_c is the minority carrier capture cross section of the said defects. The introduction rate k is evaluated using the atomic theory for displacement under electron radiation, and the calculation for σ_c is adapted from Henry and Lang's high-temperature multiphonon emission formulation. A linear scaling relationship is observed between k, K_L and nonionizing energy loss—validated by bibliographic data in the radiation energy range $E \approx 0.7$–12 MeV. Our model reproduces the increasing trend in K_L with doping, as observed in the literature, while also capturing the anisotropy between the p-type and n-type materials, with the p-type exhibiting greater radiation resistance than its n-type counterpart. The calculated K_L is fed into the physical model for solar cell operation to obtain the post-irradiated I_{sc}, V_{oc}, P_{max} at a given fluence Φ. The degradation of the electrical quantities is consistent with the measurements recorded in the literature. The findings show that InGaP is more radiation resistant than GaAs. It is demonstrated that calculating k not only aids in determining the degradation of solar cell parameters from first principles, but also in obtaining the empirical function for degradation: $a - b\log(1 + ck\Phi)$, used in fitting the experimental measurements. The limitations and potential scope of improvements in the model are also discussed.

I. INTRODUCTION

The degradation in electrical performance of solar cells under particle irradiation is quantified chiefly using two methods. In the JPL (Jet Propulsion Laboratory) model, the idea is to obtain a universal degradation curve for a photovoltaic parameter with respect to the particle fluence (Φ) that is unique to a particular cell architecture. Individual degradation curves—acquired from exhaustive ground tests done over an energy range simulating the space environment—are scaled by the *critical fluence* to the 1 MeV electron irradiation curve.[1,2] Provided the knowledge of in-orbit fluence and spectral distribution, the end-of-life performance in space can be directly read off this curve. The second method, the NRL (Naval Research Laboratory) model, uses the theoretically determined metric *nonionizing energy loss (NIEL)*, which is the amount of energy lost to atomic displacements by a particle traversing the material, as a measure for relative damage (damage = NIEL ×fluence).[3,4] This approach also establishes a standard degradation curve while requiring far fewer ground tests than the former. While these semi-empirical approaches are effective at capturing overall phenomenology, they fall short of delineating the change in fundamental transport properties that underpin electrical degradation.

It is generally understood that particle irradiation generates lattice defects that manifest as deep lying traps in the bandgap. Defect-assisted recombination is the primary mechanism for deterioration of transport properties, such as carrier concentration, diffusion length, mobility, and, consequently, the overall solar cell characteristics.[5,6] Of these, degradation of minority carrier diffusion length (L_o) has the most significant impact on the current collection efficiency in a photovoltaic device.[7,8] To a first-order approximation, the rate at which the electronic properties of

semiconductors are degraded by irradiation is often expressed in terms of a damage coefficient,[9]

$$\frac{1}{L_\Phi^2} - \frac{1}{L_o^2} = \Delta\left(\frac{1}{L^2}\right) \simeq K_L \Phi, \tag{1}$$

where the suffix "o" and "Φ" indicate the pre- and post-irradiated values, respectively, and K_L is the damage coefficient. Using an approach proposed by Bourgoin and co-workers,[10,11] K_L can be calculated by combining key characteristics of the irradiation-induced traps, specifically the product of defect introduction rate k and carrier capture cross section σ_c ($k\sigma_c$), within the Shockley–Read–Hall (SRH) theory for non-radiative recombination.[12–14] The reduced diffusion length can then be directly fed into the physical model for solar cells for post-irradiation analysis.

The use of optical device simulators, such as PC1D and NanoTCAD, for modeling irradiated $In_{1-x}Ga_xP/In_{1-y}Ga_yAs/GaAs/Ge$ multijunction solar cells[15–17] has seen a rising preponderance in the community given the ease with which the transport properties can be fine-tuned and implemented in the simulations. An analytical methodology to model electrical degradation from the ground up is developed in the study by Gauffier *et al.*.[18,19] This method, however, relies on experimental techniques, such as electroluminescence or deep level transient spectroscopy (DLTS), to determine defect production and carrier capture rate. An exhaustive *ab initio* approach that bridges the change in transport properties to the change in macroscopic characteristics in an irradiated solar cell remains an open problem.

In this study, we devise an approximate first-principles method for calculating K_L pertaining to the key recombination centers. The introduction rate k is calculated from the elementary atomic displacement and cascading theory.[20–23] The analysis is carried out at room temperature conditions for GaAs and $In_{1-x}Ga_xP$ (InGaP from here on for $x = 0.51$) solar cells subjected to the radiation energy E in the range ≈0.7–12 MeV, significantly greater than twice the displacement threshold energies known for most materials.[24] In Sec. II A, we show a linear scaling relationship between the calculated damage coefficient $K_L(E)$, introduction rate $k(E)$, and the classically derived NIEL, corroborated by the literature data in the said regime. The threshold displacement energy E_d deduced from the spectrum for $K_L(E)$ is significantly greater than that reported for atomic displacements in GaAs and InGaP crystals, implying defect recombination processes at work, giving rise to an enhanced effective E_d. In Sec. II B, the carrier capture cross section σ_c for the deep levels is estimated using Henry and Lang's high-temperature multiphonon emission (MPE) formulation.[25] The model in this study allows one to compare damage coefficients for two materials of different impurity types and concentrations; in Sec. III, we observe a qualitative increase in the damage coefficient with doping density, with the p-type material exhibiting greater robustness against irradiation than their n-type counterparts—an anisotropy noted in Si and Ge semiconductors as well.[26,27] The capture cross section of defects, and thus the damage coefficient values, is found to be an order of magnitude smaller in InGaP than in GaAs. In Sec. IV, the absolute value of K_L is incorporated in a drift–diffusion based physical model governing the solar cell behavior. The I–V characteristics are re-assessed to obtain the post-irradiation maximum power point. The end-of-life performance for both cells is reproduced with reasonable accuracy, with the factor K_L (or equivalently k) lending itself to a degradation scaling function akin to *critical fluence* and *NIEL* in the JPL and NRL methods, respectively.

II. CALCULATING THE DAMAGE COEFFICIENT

The effect of a recombination center on the minority carrier lifetime τ is given by the expression[12–14]

$$\Delta\left(\frac{1}{\tau}\right) = N_t \sigma_c v f(E_t - E_f), \tag{2}$$

where σ_c is the capture cross section of the trap, v is the carrier thermal speed, and $f(E_t - E_f)$ is the trap occupation probability of the carrier with respect to the Fermi level E_f, given by the Fermi–Dirac distribution. The total number of defects, N_t, induced by electron radiation of energy E in a lattice with atomic density n_A is calculated via[28]

$$N_t = n_A \int_0^\infty \sigma(E)\phi(E)dE, \tag{3}$$

where $\sigma(E)$ is the cross section for the incoming particle to cause an atomic displacement,

$$\sigma(E) = \int_{E_d}^{T_m} \frac{d\sigma_d(E, T_r)}{dT_r} \nu(T_r) dT_r. \tag{4}$$

For electrons, σ_d is the relativistic Mott scattering cross section for energy transfer T_r ranging from E_d, the minimum threshold energy to incur atomic displacement, to T_m, the maximum recoil energy of the displaced atom. A simplified closed form for the differential was estimated by McKinley and Feshbach,[21]

$$\frac{d\sigma_d(E, T_r)}{dT_r} = 4\pi a_o^2 Z_2^2 E_R^2 \frac{(1-\beta^2)}{m_o^2 c^4 \beta^4} \times \left(1 - \beta^2 \frac{T_r}{T_m} + \frac{\pi Z_2 \beta}{137}\sqrt{\frac{T_r}{T_m}} - \frac{T_r}{T_m}\right)\frac{T_m}{T_r^2}, \tag{5}$$

where a_o is the Bohr radius, Z_2 is the target atomic number, E_R is the Rydberg constant, β is the ratio of electron velocity to the velocity of light c, and m_o is the electron mass. The term ν, discussed in depth in Subsection II A, counts the number of displacements produced per primary knock-on atom (PKA) of recoil energy T_r.

For mono-energetic radiation, Eqs. (1)–(4) can be combined and expressed as

$$K_L\Phi = \frac{n_a}{D}\int_{E_d}^{T_m} \frac{d\sigma_d(E, T_r)}{dT_r} \nu(T_r) dT_r \sigma_c v f(E_t - E_f)\Phi = \frac{k\sigma_c v_a f(E_t - E_f)}{D}\Phi,$$

where k is the defect introduction rate (cm^{-1}),

$$k(E) = n_a \int_{E_d}^{T_m} \frac{d\sigma_d(E, T_r)}{dT_r} \nu(T_r) dT_r, \tag{6}$$

and has a direct effect on the minority carrier diffusion length via the damage coefficient,

$$K_L(E) = \frac{k(E)\sigma_c \nu_a f(E_t - E_f)e}{k_b T \mu(T)}. \tag{7}$$

The factor D is the diffusion constant, related to $\mu(T)$, the minority carrier mobility at the operating temperature T via the Einstein equation (k_b is the Boltzmann constant and e the electronic charge). The minority carrier mobility is assumed to be a material constant that remains unchanged under irradiation. The study is restricted to doping concentrations less than $\approx 10^{18}$ cm^{-3} to preclude Auger recombination effects. Here, we employ a Caughey–Thomas-like empirical model for minority carrier mobility in III–V compounds, with a dependence on temperature (T) and impurity concentration (N),[29]

$$\mu(N, T) = \mu_{\min} + \frac{\mu_{\max}(300K)(300K/T)^{\theta_1} - \mu_{\min}}{1 + \left(\frac{N}{N_{\text{ref}}(300K)(T/300K)^{\theta_2}}\right)^{\lambda}}, \tag{8}$$

where θ_1, θ_2, λ, N_{ref} are material dependent fitting parameters (listed in Table I). For very low doping concentration, mobility saturates to $\mu_{\max}(T)$, the lattice limited mobility at temperature T. At a very high doping concentration limit, mobility saturates to the temperature independent constant $\mu_{\min}$. At room temperature, Eq. (8) simplifies to

$$\mu(N, 300K) = \mu_{\min} + \frac{\mu_{\max}(300K) - \mu_{\min}}{1 + \left(\frac{N}{N_{\text{ref}}(300K)}\right)^{\lambda}}. \tag{9}$$

The mobility is considered to be independent of dopant concentration, dopant species, dopant compensation, growth method, carrier–carrier/surface scattering effects, etc. Furthermore, the authors issue caution against using the model for low temperatures (<100–150 K), where the constants λ, θ_1, θ_2 may need to be parameterized as functions of temperature. Despite these limitations, the equation produces very good fits to the data for III–V materials in the temperature and concentration range of our interest.[29]

A. Introduction rate and damage coefficient scaling with NIEL

The calculation for ν employs the modified Kinchin–Pease (Norgett–Robinson–Torrens) counting model[22,23] where the number of secondary displacements by a PKA of recoil energy T_r is given as

$$\nu(T_r) = \begin{cases} 0, & T_d < E_d, \\ 1, & E_d \le T_d < \frac{2E_d}{\kappa}, \\ \frac{\kappa T_d}{2E_d}, & \frac{2E_d}{\kappa} \le T_d. \end{cases} \tag{10}$$

The pre-factor κ accounts for the *displacement efficiency* of a PKA with energy T_r and, in general, takes the value ≈ 0.8.[23] The *damage energy* T_d is used to demarcate the energy regimes in place of T_r as T_d is the actual recoil energy available for atomic displacement after accounting for the fraction lost to electronic interactions. It is expressed as $T_d = T_r L(T_r)$, where $L(T_r)$ is the Lindhard partition function[30]—the ratio of energy lost to creating atomic displacements over the total energy loss. Equation (6) can thus be rewritten as

$$\begin{aligned} k(E) = n_a &\int_{E_d}^{\frac{2E_d}{\kappa}} \frac{d\sigma_d(E, T_r)}{dT_r} dT_r \\ &+ \frac{n_a \kappa}{2E_d} \int_{\frac{2E_d}{\kappa}}^{T_m} \frac{d\sigma_d(E, T_r)}{dT_r} T_r L(T_r) dT_r. \end{aligned} \tag{11}$$

To simplify the calculation in the range $T_d \ge \frac{2E_d}{\kappa}$, the product $T_d = T_r L(T_r)$ is approximated as $\simeq T_r \overline{L}$, where $\overline{L} = \int_{E_d}^{T_m} L(T_r) dT_r / (T_m - E_d)$ is the average estimate for L at a given incident energy E, applied to all displacements in the collision cascade.

The total introduction rate k summed over all defects for GaAs at 1 MeV takes the value $\approx 0.66\ cm^{-1}$ in comparison with the $k \approx 1\ cm^{-1}$ calculated using the basic Kinchin–Pease model.[2] With the assumption that there is no significant shift in the Fermi level and no change in the minority carrier capture cross section σ_c under irradiation as posited in the study by Gauffier *et al.*,[18] the damage constant $K_L(E)$ in Eq. (7) simply scales with $k(E)$ as

$$K_L(E) = K_L(1\text{MeV}) \frac{k(E)}{k(1\text{MeV})}. \tag{12}$$

Furthermore, under the binary collision approximation, the average energy lost per unit length in a material to nonionizing processes, i.e., the NIEL, is directly proportional to the defect

TABLE I. Fitting parameters for the mobility model in Eq. (8).[29]

Material	Electron or hole	$\mu_{\max}$ (300 K) (cm^2/V s)	$\mu_{\min}$ (cm^2/V s)	N_{ref} (300 K) (cm^{-3})	λ	θ_1	θ_2
GaAs	Electron	9400	500	6×10^{16}	0.394	2.1	3.0
	Hole	491.5	20	1.48×10^{17}	0.38	2.2	3.0
$In_{0.49}Ga_{0.51}P$	Electron	4300	400	2.0×10^{16}	0.70	1.66	…
	Hole	150	15	1.5×10^{17}	0.80	2.0	…

introduction rate. The relationship can be promptly established knowing the expression for NIEL,

$$\mathrm{NIEL}(E) = \frac{N_A}{A}\int_{E_d}^{T_m}\frac{d\sigma_d(E,T_r)}{dT_r}T_rL(T_r)dT_r, \tag{13}$$

and rewritting and rearranging Eq. (11),

$$k(E) = n_a\int_{E_d}^{\frac{2E_d}{\kappa}}\frac{d\sigma_d(E,T_r)}{dT_r}dT_r + \frac{\kappa\rho}{2E_d}\frac{N_A}{A}\int_{\frac{2E_d}{\kappa}}^{T_m}\frac{d\sigma_d(E,T_r)}{dT_r}T_rL(T_r)dT_r. \tag{14}$$

For $T_d \gg \frac{2E_d}{\kappa}$, $k(E)$ can be approximated as

$$k(E) \simeq \frac{\kappa\rho}{2E_d}\mathrm{NIEL}, \tag{15}$$

where ρ is the atomic density for a zinc-blende crystal structure.

From Eqs. (12) and (15), we have three simple concomitant scaling relations between $K_L(E)$, $k(E)$, and NIEL,

$$\frac{K_L(E)}{K_L(1\,\mathrm{MeV})} = \frac{k(E)}{k(1\,\mathrm{MeV})} = \frac{\mathrm{NIEL(E)}}{\mathrm{NIEL}(1\,\mathrm{MeV})}. \tag{16}$$

Figures 1 and 2 compare the calculated K_L (dashed red) and NIEL (solid black) with the bibliographic[5,15,31,32] K_L for GaAs and InGaP, respectively, all scaled by the respective values at 1 MeV [as per Eq. (16)]. The bibliographic values of K_L (without scaling) are shown in a scatterplot, Fig. 11 in Appendix A.

The curve for scaled $K_L(E)$ in Figs. 1 and 2 agrees well with the scaled NIEL curve[33]—satisfying the relation in Eq. (15). In GaAs, the best collapse of Eqs. (15) and (16) to the experimental data is achieved for the threshold energy $E_d \simeq 25$ eV. In a previous study,[34,35] the value of E_d for a GaAs subcell is reported to be $\simeq 21$ eV. It is likely that the data are displaying partial defect recombination effects at room temperature to compensate for which the apparent threshold increases from the documented value of 10 eV[36] at 77 K to 21–25 eV at room temperature. The recombination and survival aspect of defects apparent at extreme high and low energy cannot be captured by the BCA hypothesis, but the classically computed NIEL and K_L is in accordance with the experimental data in the intermediate energy range considered here.

For InGaP, the deep level H2 (activation energy $E_v + 0.55$), attributed to the phosphorus Frenkel pair, is held responsible for carrier recombination. The threshold damage energy for phosphorus displacement, and thus for the InGaP crystal, is remarked to be in the range of ≈4–9 eV.[37–39] Such low values of E_d may reproduce the degradation behavior under low-energy electron irradiation but will lead to an overestimated account of the defect production rate when extrapolated to higher energy. Here, the best fit to the data is obtained by means of Bragg's law with threshold energies ≃42, 21, and 21 eV for In, Ga, and P, respectively. The measurements in the study by Campesato *et al.*[35] also report similar values, suggesting that although the lifetime killing defect is associated with the phosphorus displacement, recoils in all three sublattice In, Ga, and P are

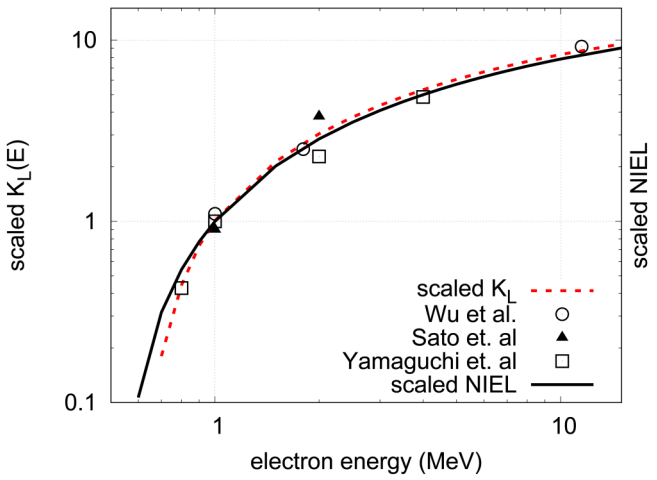

FIG. 1. Comparing the calculated damage coefficient $K_L(E)$ and the measured K_L values[5,15,31] with the NIEL for GaAs, all scaled by the respective values at 1 MeV.

important for counting defects in the super-threshold energy regime. Using independent measurements for the defect introduction rate at extreme low (closer to $2E_d$) and high incident energies (where the rise in k saturates), a molecular dynamics based approach accounting for collective atomic motion should yield an effective NIEL theory that estimates the operative E_d accurately without overcounting the defect production rate (as done for silicon by Arnolda *et al.*[40]).

B. Calculating carrier capture cross section

The recombination statistics in Eq. (2) assumes an *ad hoc* value for σ_c without delving into the microscopic theory

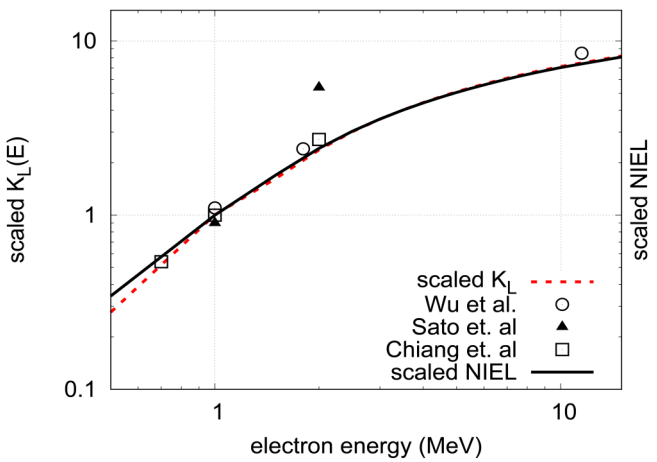

FIG. 2. Comparing the calculated damage coefficient $K_L(E)$ and the measured K_L values[15,31,32] with the NIEL for InGaP, all scaled by the respective values at 1 MeV.

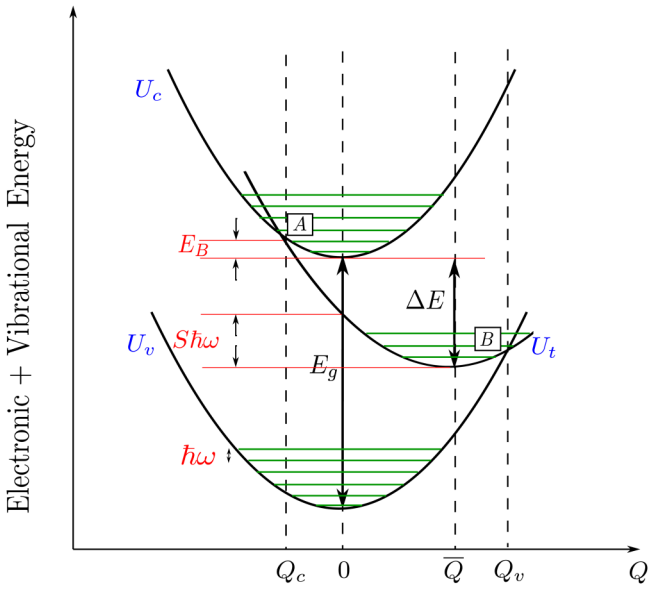

FIG. 3. Configuration coordinate diagram for the system energy (electronic +vibrational) vs the lattice coordinate Q. The labels U_c, U_t and U_v denote the potential well for the lattice when the electron is in the conduction band, the trapped state, and the valence band, respectively. E_B represents the thermal barrier against transition from U_c to U_t. The term $S\hbar\omega$ is the Franck–Condon vibrational energy shift corresponding to the offset in the equilibrium position of the potential wells participating in the transition. It is this shift that quantifies the coupling and hence the likelihood of transition between the two electronic levels. The first step, capture of a minority carrier, occurs at point A, a horizontal crossover between the two potential wells. The electronic energy is unchanged in this process, but the system is now in a vibrationally excited state. The system relaxes via phonons to its new equilibrium position $\overline{Q}$, a process much faster than the first step. The majority carrier is captured at point B, again a process much faster than the first step. The rate limiting process in the recombination of an e–h pair, thus, is the capture of a minority carrier.

underlying its origin. The capture cross section of deep defects is chiefly determined using deep level transient spectroscopy (DLTS), in which the change in junction capacitance under an injection pulse and the subsequent emission rate render important information about carrier capture for all the recombination centers in a given temperature range. There exists an exhaustive body of work characterizing defects in InGaP and GaAs under electron irradiation.[11,36,41–46] In GaAs, it is seen that the radiation-induced defects under room temperature 1 MeV radiation are principally primary in nature,[47] comprising a V_{As}–As_i vacancy–interstitial pair in the As sublattice. Among the non-native, irradiation-induced traps, the electron trap E5 at $E_c-0.96$ in p-GaAs and hole trap H1 at $E_v+0.3$ in n-GaAs are the most effective recombination centers for fluence levels above $\approx 10^{15}$ cm^{-2}.[48,49] In InGaP solar cells, deep level H2 at $E_v+0.55$ (electron/hole trap in n/p-InGaP), speculated as a phosphorus Frenkel pair, is the purported lifetime killer.[50]

Non-radiative recombination facilitated by deep levels corresponding to point defects is understood to occur via the multiphonon emission (MPE) mechanism.[25,51–54] The defects in these systems cause a large lattice distortion, which manifests in a strong coupling between the defect state and the lattice neighborhood. An electron is captured provided sufficiently large lattice vibrations induce crossings between a free state in the conduction band and the localized trap state. Following the capture, the lattice around the defect having received the net energy relaxes about its new equilibrium position, emitting phonons that propagate away from the defect site. The process can be best understood by a configuration coordinate diagram (see Fig. 3) (say, for a capture of a minority electron by a neutral defect state from the conduction band).

The theoretical treatment of MPE capture for defects in GaAs began with the seminal work of Henry and Lang,[25] where they use first-order perturbation theory to calculate the transition rate between the bulk and trap states around the level crossing region. In the strong lattice coupling and high-temperature limit, they arrive at the closed form,

$$\sigma_c = \sigma_\infty e^{-E_B/k_bT}, \tag{17}$$

where the activation barrier E_B is the thermal energy in the lattice necessary to reach the crossing point between U_c to U_t, given by

$$E_B = \frac{(\Delta E - S\hbar\omega)^2}{4S\hbar\omega}, \tag{18}$$

with ΔE being the energy difference between the trap and minority band. The factor $S\hbar\omega$, the Franck–Condon (FC) shift, represents the strength of electron–lattice coupling with $\hbar\omega$ being the quanta of phonon energy and S being the Huang–Rhys factor, quantifying the number of phonons emitted in the relaxation following the capture. A strong FC shift (the upper bound for which is ΔE, corresponding to the crossover point A at $Q=0$) yields a lower thermal barrier and higher lattice relaxation energy, making the carrier capture an energetically favorable process. Hence, the likelihood of the transition enhances with a higher value of $S\hbar\omega$.

The calculation for the prefactor σ_∞ reduces to evaluating the matrix element $\langle t|\Delta V|c\rangle$ in

$$\sigma_\infty = \sqrt{\frac{\pi}{S\hbar\omega kT}}\frac{\Omega|\langle t|\Delta V|c\rangle|^2}{\hbar\nu}, \tag{19}$$

where $|t\rangle$, $|c\rangle$ are the electronic states for the electron in the trapped state and a free state in the conduction band, respectively, Ω is the volume of the unit crystal, and ΔV is the perturbation in electronic potential that causes transitions between the electronic states about the crossing point. The defect and nearest-neighbor form a spherical potential well, binding the electron at a state $\epsilon_1 = E_c - E_t(Q_1)$ below the free state continuum. The wavefunctions are assumed to be independent of Q in the region $|Q-Q_c| < Q_1$, only a function of the electronic coordinate of the potential well. Solving for the spherical wavefunctions (cf. Sec. III D of Ref. 25), they arrive at $\Omega|\langle t|\Delta V|c\rangle|^2 \approx 2\pi a^3\epsilon_1$, where a is the radius of the bound state given by $a=\sqrt{\hbar^2/2m^*\epsilon_1}$. The value ϵ_1 was rigorously shown to be ≈ 0.06 eV. Using $\nu=\sqrt{\frac{8k_bT}{\pi m^*}}$ where m^* is

TABLE II. Main recombination centers induced by 1 MeV electron irradiation. Comparison between the calculated and experimental values for $k(\mathrm{cm}^{-1})$, $\sigma_c(\mathrm{cm}^2)$, and $k\sigma_c(\mathrm{cm})$.

Defects	E (eV)	k (exp)	k (calc)	σ_c (exp)	σ_c (calc)	$k\sigma_c$ (exp)	$k\sigma_c$ (calc)
GaAs							
E5	E_c −0.96	0.1 (Ref. 11) 0.04 (Ref. 49) 0.1 (Ref. 46)	0.66	1.8×10^{-12} (Ref. 11) 7×10^{-13} (Ref. 49) 5.3×10^{-12} (Ref. 46) 1×10^{-13} (Ref. 45)	1×10^{-13}	1.8×10^{-13} 1×10^{-14} (Ref. 18)	6.6×10^{-14}
H1	E_v +0.3	0.1–0.7 (Ref. 11)	0.66	0.5×10^{-14} (Ref. 11)	1.2×10^{-13}	3.5×10^{-15}	8×10^{-14}
InGaP							
H2	E_v +0.55	0.093 (Ref. 46) 0.1 (Ref. 11)	0.63	2.9×10^{-13} (Ref. 46) 1.8×10^{-12} (Ref. 11)	2.6×10^{-14}	2.7×10^{-14} $1–10\times10^{-14}$ (Ref. 18)	1.6×10^{-14}

the effective mass of the minority carrier, we have

$$\sigma_\infty = \sqrt{\frac{\epsilon_1}{S\hbar\omega}}\frac{\pi^2}{4k_bT}\frac{\hbar^2}{m^*}. \tag{20}$$

Therefore, the strong coupling, high-temperature capture cross section achieves the form

$$\sigma_c = \sqrt{\frac{\epsilon_1}{S\hbar\omega}}\frac{\pi^2}{4k_bT}\frac{\hbar^2}{m^*}e^{-E_B/k_bT}, \tag{21}$$

where the FC shift, $S\hbar\omega$, and activation energy E_B are the unknowns pertaining to the defect in question, both quantities related via Eq. (18). The first-principles derivation of an FC shift is outside the scope of this study. On the contrary, we use experimentally determined FC shifts for the key defects in GaAs and InGaP found in the literature so far. In the study by Fleming *et al.*,[55] one of the objectives was to fit their experimental data to the known form of a zero field trapping rate coefficient for two hole and three electron defects at 300 K. The best estimate for $S\hbar\omega$ in the case of E5 was deduced to be around ≈0.25–0.3 eV, which when substituted in Eq. (17) for σ_c gives an estimate of $\approx1\times10^{-13}$ cm^2 for E5 ($m^*=0.06m_o$, $S\hbar\omega=0.3$ eV[55]). For H1 ($m^*=0.08m_o$, $S\hbar\omega=0.36$ eV[55]), we get $\sigma_c\approx1.2\times10^{-13}$ cm^2. As for InGaP, an analytical or semi-empirical treatment delineating the MPE capture by H2 remains an open area of interest. The reported σ_c for H2 lies in the rather large range of 10^{-16}–10^{-13} cm^{-2}.[11,18,43,46] Considering a typical value of strong coupling factor S in the range ≈10–15,[56] say $S\simeq12$, and a room temperature vibrational frequency of $\hbar\omega_o\simeq25$ meV, the value of E_b comes around ≃0.052 eV (compared to $E_B\simeq0.06$ eV reported by Khan *et al.*[44]). Using this, we obtain an approximate value for $\sigma_c\simeq2.6\times10^{-14}$ cm^2.

The calculated σ_c in the present work is compared with the experimentally deduced cross section values in Refs. 11, 45, 46, and 49 (see Table II). The calculated value of σ_c for the H2 defect in InGaP is smaller by an order of magnitude than that for the defects in GaAs. The calculated σ_c in this study is a slight underestimate when compared to measured values. This is the limitation of the high temperature approximation in Eq. (21), which deviates from the quantum-mechanically calculated capture cross section at low temperatures ($k_bT<\hbar\omega_o$) where tunneling effects are more important than activation (cf Fig. 4 in Ref. 56). The calculated k on the other hand is a slight overestimate when compared to the measured k, especially for the case of H2 in InGaP. The reason for this is discussed in Subsection II A: our model for evaluating the defect production rate does not account for the room temperature defect annealing process, resulting in an overcount of net defects created.

The product $k\sigma_c$ will be employed in Eq. (7) to evaluate K_L in Sec. III. We shall see that despite the approximations, the evaluated $k\sigma_c$ faithfully reproduces the experimentally measured K_L for a large range of doping density.

III. K_LS VS DOPANT-TYPE AND CONCENTRATION

Combining the calculations in Subsections II A and II B in the expression given in Eq. (7), K_L is evaluated for GaAs and InGaP under 1 MeV electron irradiation at room temperature in both p-type, n-type subcells. Figures 4 and 5 show the increasing trend in K_L with increasing doping levels. The analysis is restricted to doping concentration $N_d\geq10^{15}$ cm^{-3}, where any effect of series resistance caused by low carrier concentration can be safely neglected. In the doping regime of 10^{15}–10^{19} cm^{-3}, the calculated K_L lies in the range of 1.2×10^{-7}–6×10^{-7} for n-GaAs and 1.4×10^{-8}–7.2×10^{-8} for p-GaAs, while it varies from 5.5×10^{-8}–4×10^{-7} for n-InGaP and 6×10^{-9}–5×10^{-8} for p-InGaP, respectively. Overall, InGaP solar cells display more favorable damage coefficient than GaAs cells—by almost an order of magnitude. It is also noted that p-GaAs and p-InGaP are more radiation resistant than their n-type counterparts, as evident from the experimental data.

For GaAs, this difference of behavior in p- and n- type material can be mainly attributed to the difference in mobility of interstitial arsenic (As_i) under irradiation. The vacancy–interstitial pair V_{As}–As_i is more tightly bound in n- type than in p- type GaAs, where the interstitial arsenic forms complexes with impurities that are not pertinent to lifetime degradation.[42,57,58] This dopant-type dependency of radiation hardness is also apparent in Si and Ge solar cells. For Si, the capture of free minority electrons destabilizes the FP in p-Si, resulting in a higher rate of annihilation of defects

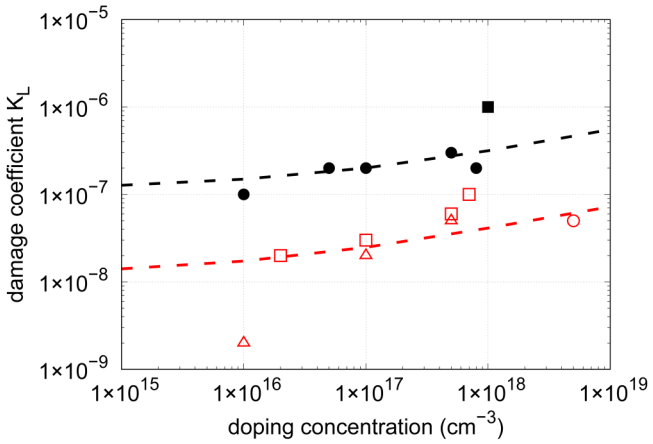

FIG. 4. Comparing damage coefficient for an n/p GaAs cell with doping concentration under 1 MeV electron irradiation. Data in red and black correspond to *p*- and *n*-type respectively. Dashed lines represent the calculation in this work, and scatter data are taken from references: □, ■,[62] ●,[63] ●,[63] and △.[64]

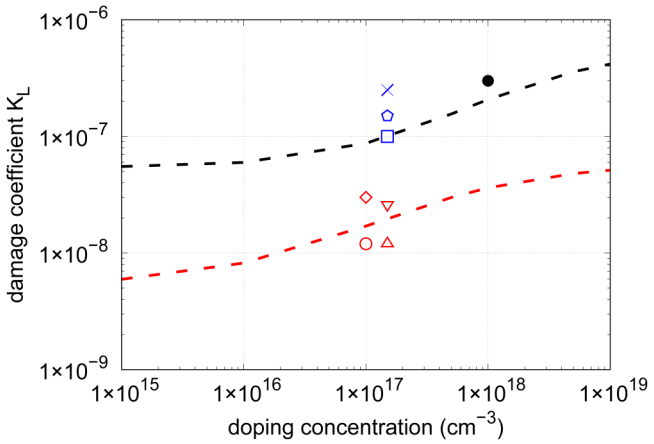

FIG. 5. Comparing damage coefficient for *n*- and *p*- InGaP cells with doping concentration. Data in red and black correspond to *p*- and *n*- type, respectively. Points in blue are measured values for InGaP *n*+*p* solar cells, plausibly limited by the more degradable *n*-layer. Dashed lines represent the calculation in this work, and scattered data are taken from references: ×,[15] □,[31] ⬠,[50] ●, ◇,[32] ▽,[65] ●,[66] and △.[67]

than in *n*-Si.[59] In Ge too, owing to a similar effect, the FP is very unstable in general but more so in *p*-Ge than in *n*-Ge.[27]

For InGaP as well, the trend indicates higher robustness against radiation in the case of *p*-InGaP-supported by the observation that minority carrier injection in an *n*+*p* solar cell annealed most defects, leading to a recovery of the electrical performance comparable to the pre-irradiated values[32,60] whereas only partial recovery was observed in a *p*+*n* solar cell[61] under minority carrier injection.

IV. CALCULATING SOLAR CELL DEGRADATION

The validity of the K_L calculations is finally assessed by comparing the degraded photovoltaic characteristics computed using the formulation in Appendix B, with the corresponding experimental measurements. The analysis is conducted for bare single junction *n*+*p* GaAs (*n*-emitter, $N_D = 2 \times 10^{18}$ cm^{-3}, *p*-base, $N_A = 1 \times 10^{17}$ cm^{-3}) and InGaP (*n*-emitter, $N_D = 2 \times 10^{18}$ cm^{-3}, *p*-base, $N_A = 3 \times 10^{17}$ cm^{-3}) solar cells under AM0 illumination. The analysis neglects any surface/interface recombination phenomena while retaining only the effect of degraded minority carrier lifetime,

$$L_{n/p} = \frac{L_{n0/p0}}{\sqrt{1 + \phi K_{Ln/Lp} L_{n0/p0}^2}}, \tag{22}$$

where $L_{n/p}$ and $L_{n0/p0}$ are the pre- and post-irradiated minority carrier diffusion length for *p*- and *n*- layer, respectively, while $K_{Ln/Lp}$ denotes the damage coefficients as calculated in Sec. III. The values for the material parameters and pre-irradiated transport properties are taken from the classic text by Hovel.[68] Figure 6 juxtaposes qualitative behavior of pre- and post-irradiated IV for GaAs and InGaP solar cells for a given fluence.

Figures 7 and 8 show the universal degradation curve of the maximum power point (P_{max}), normalized by pre-irradiation values. The fluence Φ is scaled by the defect introduction rate $k(E)$ at the given particle energy (here 0.7, 1, and 3 MeV) resulting in the collapse of all degradation curves to the universal function (red dashed). Despite the simplistic approximations in modeling the I–V, a good agreement is observed with the data published by Campesato *et al.*[35] The degradation curve of electrical quantities takes the form $a - b\log(1 + ck(E)\Phi)$, where constants *a*, *b*, *c* define a given material and the degradation of the electrical parameter of the said material under radiation. The "knee" in the curve before transitioning to the logarithmically decaying regime—given by the

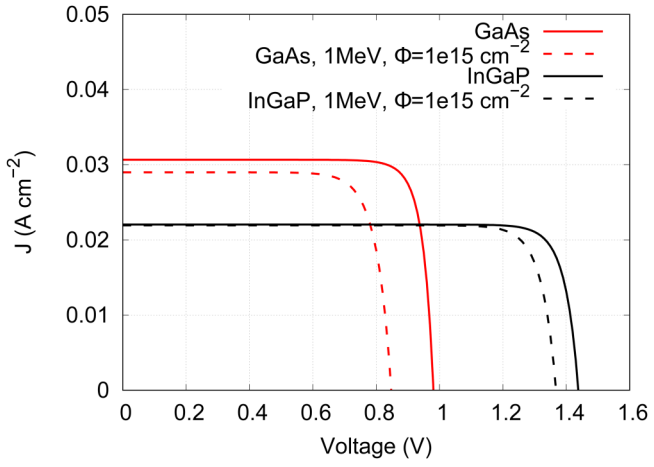

FIG. 6. Pre- and post-irradiated IV characteristics for InGaP and GaAs solar cells under AM0 illumination.

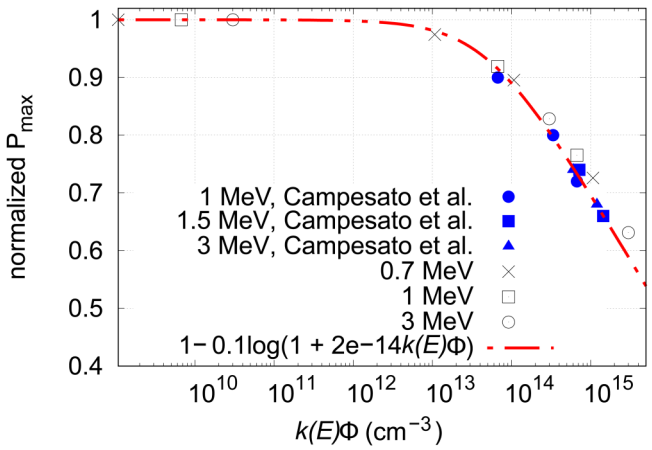

FIG. 7. Normalized P_{max} vs scaled fluence $k(E)\Phi$ for a GaAs solar cell. The experimentally measured values[35] are also scaled by $k(E)$ calculated in this study. The analytically calculated values agree well with the experimental data—both of them satisfying the functional form stated in the legend.

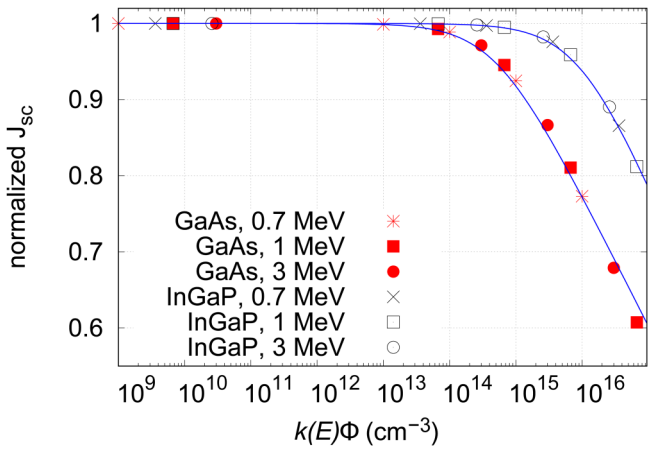

FIG. 9. Normalized J_{sc} vs scaled fluence $k(E)\Phi$ for GaAs and InGaP solar cells. The points represent values calculated in this study. Both curves satisfy the functional form $a - b\log(1 + ck(E)\Phi)$ (solid blue lines). InGaP displays a distinctively favorable critical fluence value at the "knee" $(1/c)$ than GaAs.

pre-factor $1/c$—is achieved in InGaP at a fluence value greater than GaAs, suggesting a lower limit for the critical fluence (beyond which damage increases logarithmically) in GaAs than that in InGaP, while the rate of degradation with fluence in the logarithmic region—given by the slope b—for InGaP is lesser than that for GaAs. These observations demonstrate the superior radiation hardness of InGaP cells over GaAs. Figures 9 and 10 show the universal degradation curves for J_{sc}, the short circuit current density, and V_{oc}, the open circuit voltage in GaAs and InGaP cell, respectively, further confirming the marked difference in the response to radiation in InGaP and GaAs solar cells. Figures 7–10 substantiate the applicability of the defect introduction rate, $k(E)$, as a scaling factor in lieu of NIEL to quantify displacement damage as the two quantities have a linear correlation in the intermediate radiation energy range as seen in Sec. II A.

V. DISCUSSION AND CONCLUSION

The computation of K_L for an electron-irradiated solar cell in this study could be a viable addition to device modeling simulators. In fact, the formulation described in Appendix B is sufficient to

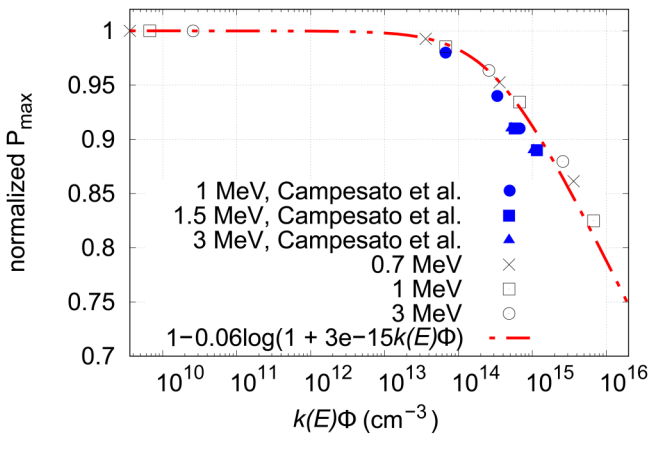

FIG. 8. Normalized P_{max} vs scaled fluence $k(E)\Phi$ for an InGaP solar cell. The experimentally measured values[35] are also scaled by $k(E)$ calculated in this study. The analytically calculated values agree well with the experimental data—both of them satisfying the functional form stated in the legend.

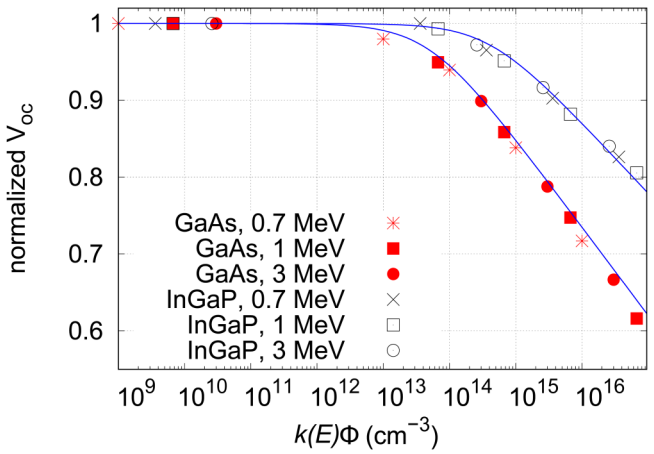

FIG. 10. Normalized V_{oc} vs scaled fluence $k(E)\Phi$ for GaAs and InGaP solar cells. The points represent values calculated in this study. Both curves satisfy the functional form $a - b\log(1 + ck(E)\Phi)$ (solid blue lines). InGaP displays a distinctively favorable critical fluence value at the "knee" $(1/c)$ and a lower rate of degradation (b) than GaAs.

estimate the degraded IV and end-of-life performance of solar cells. A non-trivial limitation of this calculation is its applicability only under the premises where the lifetime killing traps pertain to lattice defects that are principally primary in nature, with a concentration growth proportional to fluence, and do not combine with other defects or impurities to form secondary complexes. For instance, in indium phosphide (InP) solar cells, it is observed that K_L decreases with doping density, with the n-InP material by and large displaying greater radiation hardness than p-InP. This effect is ascribed to the transformation of the damaging defect H(0.32), a primary type in the phosphorus sublattice, to an otherwise docile defect H(0.52), which shows an increase in concentration with the doping density—alluding to a defect-impurity complex identity of the transformed defect.[6,69]

This work complements the study done by Gauffier *et al.*[18,19] where a power law dependence of the product $k\sigma_c$ on NIEL was experimentally deduced and implemented in their analysis. As suggested in their closing remarks, an independent calculation for the introduction rate k should dispense the need for repeated experiments in quantifying degradation since σ_c remains practically unchanged with irradiation energy.

We have calculated $k(E)$ and demonstrated its linear correlation with NIEL in the intermediate energy range of 0.7–12 MeV, validated by literature data. However, (since the calculation does not take into consideration any recombination-enhanced annealing effects) to accurately infer the displacement threshold energy from the low-energy end of the spectrum while simultaneously yielding a correct estimate of defect production rate at the high-energy end, a molecular dynamics (MD) aided effective NIEL theory for GaAs and InGaP is in order (see for Si[40]). Such a theory would also incorporate the universal anisotropy observed in defect annihilation processes between p-and n-type semiconductors. Calculating the non-radiative capture cross sections for radiation-induced defects in GaAs and InGaP from first principles is a future scope for study.

It is worth noting that the calculated $k(E)$ in this study validates itself because the analytically quantified degradation of $P_{\max}$, evaluated by incorporating the calculated $k(E)$ in the physical model for solar cell, matches exactly with the empirical function $a - b\log(1 + ck(E)\Phi)$ (like in the NRL model) representing the degradation behavior—a function that also requires the calculated scaling factor $k(E)$ as input at a given energy. Both approaches are consistent with one another and with the experimental data. The knowledge of the constants a, b, c, and $k(E)$ is sufficient to define a given material and its electrical response to radiation, independent of architecture or design. The model also shows how InGaP solar cells outperform GaAs in terms of radiation resistance: the capture cross section value of lifetime killing recombination centers in InGaP is an order of magnitude lower than in GaAs. This difference is reflected in InGaP cells having a lower K_L and a higher critical fluence value than GaAs cells—sby an order of magnitude. These inferences are backed by the bibliographic data.

AUTHOR DECLARATIONS

Conflict of Interest

The author declares no conflict of interest.

DATA AVAILABILITY

The data that support the findings of this study are available within the article.

APPENDIX A: EXPERIMENTAL MEASUREMENTS OF K_L

Figure 11 shows the absolute values of K_L for GaAs and InGaP solar cells for a range of radiation energies as measured in independent studies.[5,15,31,32] The significant scatter in the data can be ascribed to technological biases singular to an experiment, precluding any meaningful comparison between the damage coefficients of GaAs and InGaP. The scaling removes the scatter, and all the experimentally measured values fall on a single collapsed spectrum, shown in dashed lines in Figs. 1 and 2. The absolute K_L measurements differ from one study to the next, but the scaled K_L spectrum is reproducible across all studies.

APPENDIX B: MODELING IV CHARACTERISTICS

The output current density for a solar cell is given by

$$J(V) = (J_{ph} - J_{dark})(V), \tag{B1}$$

where J_{ph} is the photocurrent and J_{dark} is the sum of injective and recombination current. The total photocurrent density, J_{ph}, is the sum of the minority carrier current from the base, emitter, and depletion region, given by

$$J_{ph} = J_n + J_p + J_{dr}, \tag{B2}$$

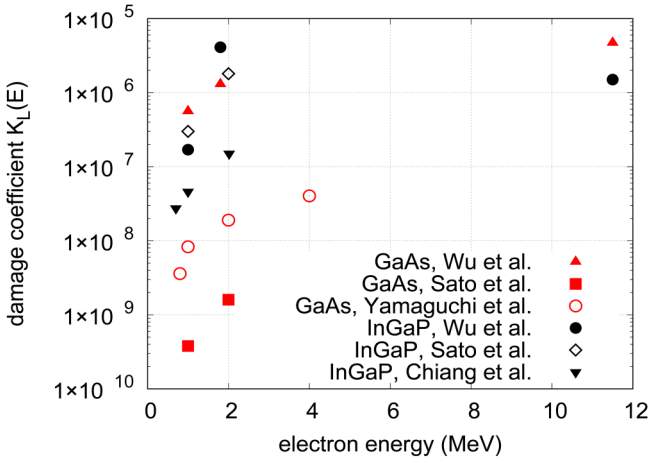

FIG. 11. The experimentally measured absolute values of diffusion length damage coefficient K_L with respect to electron energy.[5,15,31,32]

$$J_n = \frac{qF(1-R)\alpha L_n}{\alpha^2 L_n^2 - 1}\exp(-\alpha(x_j+W)) \times \left[\alpha L_n. - \frac{\frac{S_n L_n}{D_n}(\cosh\frac{H'}{L_n} - \exp(-\alpha H')) + \sinh\frac{H'}{L_n}}{\frac{S_n L_n}{D_n}\sinh\frac{H'}{L_n} + \cosh\frac{H'}{L_n}} + \frac{\alpha L_n \exp(-\alpha H')}{\frac{S_n L_n}{D_n}\sinh\frac{H'}{L_n} + \cosh\frac{H'}{L_n}}\right], \quad \text{(B3)}$$

$$J_p = \frac{qF(1-R)\alpha L_p}{1-\alpha^2 L_p^2}\left[\alpha L_p \exp(-\alpha x_j). - \frac{\left(\frac{S_p L_p}{D_p} + \alpha L_p\right) - \exp(-\alpha x_j)\left(\frac{S_p L_p}{D_p}\cosh\frac{x_j}{L_p} + \sinh\frac{x_j}{L_p}\right)}{\frac{S_p L_p}{D_p}\sinh\frac{x_j}{L_p} + \cosh\frac{x_j}{L_p}}\right], \quad \text{(B4)}$$

$$J_{dr} = qF(1-R)\exp(-\alpha x_j)[1-\exp(-\alpha W)], \quad \text{(B5)}$$

$$J_{dark} = J_{inj} + J_{rg}, \quad \text{(B6)}$$

where $F, R, \alpha, S, L, D, x_j, W, H, (H' = H - (x_j + W))$ is the number of incident photons/cm^2/s/unit bandwidth, reflectance, absorption coefficient, surface recombination velocity, minority carrier diffusion length, diffusion constant, junction edge, width of the depletion region, and width of the entire cell, respectively. The photocurrent is integrated over the entire spectrum (here, AM0, 1346 W cm^{-2}) to get the total output. The dark current density is given by

with

$$J_{inj} = \left[q\frac{D_p n_i^2}{L_p N_d}\tanh\frac{x_j}{L_p} + q\frac{D_n n_i^2}{L_n N_a}\tanh\frac{H'}{L_n}\right] \times (\exp(qV_j/kT) - 1),$$

$$J_{rg} = \frac{qn_i W}{\sqrt{\tau_{p0}\tau_{n0}}}\frac{2\sinh(qV_j/2kT)}{q(V_d - V_j)/kT}\frac{\pi}{2},$$

and τ_{p0}, τ_{n0} are the Shockley–Hall–Read (SHR) lifetimes in the base and emitter, respectively.

REFERENCES

[1]H. Y. Tada, J. R. Carter, B. E. Anspaugh, and R. G. Downing, *The Solar Cell Radiation Handbook*, 3rd ed. (JPL Publication, 1982), pp. 69–82.
[2]B. E. Anspaugh, *GaAs Solar Cell Radiation Handbook* (JPL Publication, 1996), Vol. 96–99.
[3]G. P. Summers, R. J. Walters, M. A. Xapsos, E. A. Burke, S. R. Messenger, P. Shapiro, and R. L. Statler, *IEEE Proceedings of the 1st World Conference on Photovoltaic Energy Conversion* (IEEE, 1994), pp. 2068–2073.
[4]S. R. Messenger, G. P. Summers, E. A. Burke, R. J. Walters, and M. A. Xapsos, Prog. Photovolt.: Res. Appl. **9**, 103–121 (2001).
[5]M. Yamaguchi and C. Amano, J. Appl. Phys. **54**, 5021 (1983).
[6]M. Yamaguchi and K. Ando, J. Appl. Phys. **63**, 5555 (1988).
[7]M. Yamaguchi and C. Amano, J. Appl. Phys. **58**, 3601 (1985).
[8]M. Yamaguchi, Sol. Energy Mater. Sol. Cells **68**, 31–53 (2001).
[9]C. Leroy and P. G. Rancoita, *Principles of Radiation Interaction in Matter and Detection*, 2nd ed. (World Scientific, 2009).
[10]J. C. Bourgoin and N. de Angelis, Sol. Energy Mater. Sol. Cells **66**, 467–477 (2001).
[11]J. C. Bourgoin and M. Zazoui, Semicond. Sci. Technol. **7**, 453–460 (2002).
[12]R. N. Hall, Phys. Rev. **87**, 387 (1952).
[13]W. Shockley and W. T. Read, Phys. Rev. **87**, 835 (1952).
[14]J. J. Loferski and P. Rappaport, Phys. Rev. **111**, 432 (1958).
[15]S. Sato, T. Ohshima, and M. Imaizumi, J. Appl. Phys. **105**, 044504 (2009).
[16]S. Sato, H. Miyamoto, M. Imaizumi, K. Shimazaki, C. Morioka, K. Kawano, and T. Ohshima, Sol. Energy Mater. Sol. Cells **93**, 768–773 (2009).
[17]M. Turowski, T. Bald, A. Raman, A. Fedoseyev, J. H. Warner, C. D. Cress, and R. J. Walters, IEEE Trans. Nucl. Sci. **60**, 2477 (2013).
[18]A. Gauffier, J.-P. David, O. Gilard, T. Nuns, C. Inguimbert, and A. Balocchi, IEEE Trans. Nucl. Sci. **56**, 2237 (2009).
[19]A. Gauffier, J. P. David, and O. Gilard, J. Microelectron. Rel. **48**, 1494–1499 (2008).
[20]F. Seitz and J. S. Koehler, *Solid State Physics* (Academic, New York, 1956), Vol. 2, p. 305.
[21]W. A. McKinley, Jr. and H. Feshbach, Phys. Rev. **74**, 1759 (1948).
[22]G. W. Kinchin and R. S. Pease, Rep. Progr. Phys. **18**, 1 (1955).
[23]M. J. Norgett, M. T. Robinson, and I. M. Torrens, Nucl. Eng. Des. **33**, 50–54 (1975).
[24]P. Jung, "Production of atomic defects in metals," in *Crystal and Solid State Physics*, Vol. 25 of Landolt-Bornstein, New Series III, edited by H. Ullmaier (Springer, Berlin, 1991), pp. 1–86.
[25]C. H. Henry and D. V. Lang, Phys. Rev. B **15**, 989 (1977).
[26]H. Flicker, J. Loferski, and J. Scott-Monck, Phys. Rev. **128**, 2557 (1962).
[27]A. Mesli, L. Dobaczewski, K. B. Nielsen, V. Kolkovsky, M. C. Petersen, and A. N. Larsen, Phys. Rev. B **78**, 165202 (2008).
[28]J. S. Koehler and F. Seitz, Discuss. Faraday Soc. **31**, 45 (1961).
[29]M. Sotoodeh, A. H. Khalid, and A. A. Rezazadeh, J. Appl. Phys. **87**, 2890 (2000).
[30]J. Lindhard, V. Neilson, M. Scharff, and P. V. Thomsen, Mat. Fys. Medd. Dan. Vid. Selsk. **33**, 1–42 (1963).
[31]R. Wu, J.-L. Wang, G. Yan, and R. Wang, Chin. Phys. Lett. **35**, 046101 (2018).
[32]P. K. Chiang, P. S. Vijayakumar, and B. T. Cavicchi, *Space Power Systems, Proceedings of the 23rd IEEE Photovoltaic Specialists Conference* (IEEE, 1993), p. 659.
[33]M. J. Boschini, P. G. Rancoita, and M. Tacconi, SR-NIEL calculator, "Screened Relativistic (SR) Treatment for Calculating the Displacement Damage and Nuclear Stopping Powers for Electrons, Protons, Light- and Heavy- Ions in Materials," version 7.6.1, INFN-Sezione di Milano Bicocca, Italy; see http://www.sr-niel.org/.
[34]C. Baur, M. Gervasi, P. Nieminen, S. Pensotti, P. G. Rancoita, and M. Tacconi, "NIEL dose dependence for solar cells irradiated with electrons and protons," arXiv:1312.0402 (2013).
[35]R. Campesato, C. Baur, M. Casale, M. Gervasi, E. Gombia, E. Greco, A. Kingma, P. G. Rancoita, D. Rozza, and M. Tacconi, in *Proceedings of the 35th European PV Solar Energy Conference* (WIP, 2018), pp. 959–964.
[36]D. Pons, P. M. Mooney, and J. C. Bourgoin, J. Appl. Phys. **51**, 2038 (1980).
[37]M. Imaizumi, C. Morioka, T. Sumita, T. Ohshima, and S. Okuda, in *Proceedings of the 37th IEEE Photovoltaic Specialists Conference* (IEEE, 2011), pp. 1579–1582.
[38]J. Insoo, W. Kim, and R. Evans, IEEE Trans. Nucl. Sci. **56**, 3229 (2009).
[39]Y. Okuno, S. Okuda, M. Akiyoshi, T. Oka, M. Harumoto, K. Omura, S. Kawakita, M. Imaizumi, S. R. Messenger, K. H. Lee, and M. Yamaguchi, J. Appl. Phys. **122**, 114901 (2017).
[40]P. Arnolda, C. Inguimbert, T. Nuns, and C. Boatella-Polo, IEEE Trans. Nucl. Sci. **58**, 756 (2011).
[41]D. V. Lang and L. C. Kimerling, Phys. Rev. Lett. **33**, 489 (1974).

[42]D. Pons and J. C. Bourgoin, J. Phys. C: Solid State Phys. **18**, 3839 (1985).
[43]A. Khan, M. Yamaguchi, J. C. Bourgoin, and T. Takamoto, J. Appl. Phys. **91**, 2391 (2002).
[44]A. Khan, M. Yamaguchi, N. Dharmaso, J. C. Bourgoin, K. Ando, and T. Takamoto, Jpn. J. Appl. Phys. **41**, 1241 (2002).
[45]B. A. Danilchenko, A. P. Budnyk, L. I. Shpinar, I. I. Yaskovets, K. W. J. Barnham, and N. J. Ekins-Daukes, Sol. Energy Mater. Sol. Cells **95**, 2551–2556 (2011).
[46]G. Yan, J.-L. Wang, J. Liu, Y.-Y. Liu, R. Wu, and R. Wang, J. Lumin. **219**, 116905 (2019).
[47]D. V. Lang, R. A. Logan, and L. C. Kimerling, Phys. Rev. B **15**, 4874 (1977).
[48]S. S. Li, P. M. Wang, R. Y. Loo, and W. P. Rahilly, Solid State Electron. **26**, 835–840 (1983).
[49]B. Danilchenko, A. Budnyk, L. Shpinar, D. Poplavskyy, S. E. Zelensky, K. W. J. Barnham, and N. J. Ekins-Daukes, Sol. Energy Mater. Sol. Cells **92**, 1336–1340 (2008).
[50]M. Yamaguchi, C. Vargas-Aburto, S. J. Taylor, M.-J. Yang, T. Takamoto, E. Ikeda, H. Kurita, M. Ohmori, R. M. Uribe, D. Brinker, and D. A. Scheimans, in *Proceedings of the 25th IEEE Photovoltaic Specialists Conference* (IEEE, 1996), pp. 13–17.
[51]K. Huang and A. Rhys, Proc. R. Soc. London, Ser. A **204**, 406 (1950).
[52]R. Kubo and Y. Toyozawa, Prog. Theor. Phys. **13**, 160 (1955).
[53]B. K. Ridley, J. Phys. C: Solid State Phys. **11**, 2323 (1978).
[54]T. Markvart, J. Phys. C: Solid State Phys. **14**, L895 (1981).
[55]R. M. Fleming, S. M. Myers, W. R. Wampler, D. V. Lang, C. H. Seager, and J. M. Campbell, J. Appl. Phys. **116**, 013710 (2014).
[56]A. Alkauskas, M. D. McCluskey, and C. G. Van de Walle, J. Appl. Phys. **119**, 181101 (2016).
[57]D. Stievenard, X. Boddaert, and J. C. Bourgoin, Phys. Rev. B **34**, 4048 (1986).
[58]D. Stievenard, X. Boddaert, J. C. Bourgoin, and H. J. von Bardeleben, Phys. Rev. B **41**, 5271 (1990).
[59]M. J. Beck, L. Tsetseris, M. Caussanel, R. D. Schrimpf, D. M. Fleetwood, and S. T. Plantelides, IEEE Trans. Nucl. Sci. **53**, 1372–1379 (2006).
[60]A. Khan, M. Yamaguchi, J. C. Bourgoin, K. Ando, and T. Takamoto, J. Appl. Phys. **89**, 4263 (2001).
[61]R. J. Walters, M. A. Xapsos, H. L. Cotal, S. R. Messenger, G. P. Summers, P. R. Sharps, and M. L. Timmons, Solid-State Electron. **42**, 1747 (1998).
[62]K. A. Bertness, B. T. Cavicchi, S. R. Kurtz, J. M. Olson, A. E. Kibbler, and C. Kramer, in *Proceedings of the 22rd IEEE Photovoltaic Specialists Conference* (IEEE, 1991), p. 1582.
[63]M. Yamaguchi and C. Uemura, J. Appl. Phys. **57**, 604 (1985).
[64]D. Flood and H. Brandhorst, in *Current Topics in Photovoltaics* (Academic, London, 1987), Vol. 2, p. 143.
[65]A. Khan, M. Yamaguchi, T. Takamoto, N. de Angelis, and J. C. Bourgoin, J. Cryst. Growth **210**, 264–267 (2000).
[66]M. Zazoui, M. Mbarki, A. Zin Aldin, J. C. Bourgoin, O. Gilard, and G. Strobl, J. Appl. Phys. **93**, 5080 (2003).
[67]M. Yamaguchi, T. Sasaki, H.-S. Lee, C. Morioka, N. J. Ekins-Daukes, M. Imaizumi, T. Takamoto, and T. Ohshima, *33rd IEEE Photovoltaic Specialists Conference* (IEEE, 2008), pp. 1–4.
[68]H. J. Hovel, Semicond. Semimet. Sol. Cells **11**, 14 (1961).
[69]K. Ando, M. Yamaguchi, and C. Uemera, Phys. Rev. B **34**, 3041 (1986).